Applied Surface Science 527 (2020) 146933

Contents lists available at ScienceDirect

Applied Surface Science

journal homepage: www.elsevier.com/locate/apsusc

Effect of multiple-step annealing on the structural, optical and electrical properties of ZnO:In-N films

Xiaoyu Zhang[a], Guoping Qin[a,*], Hong Zhang[a], Wanjun Li[a], Haibo Ruan[b], Liang Fang[c], Cunzhu Tong[d], Chunyang Kong[a]

[a] Chongqing Key Laboratory of Photo-Electric Functional Materials, College of Physics and Electronic Engineering, Chongqing Normal University, Chongqing 401331, People's Republic of China
[b] Research Center for Materials Interdisciplinary Sciences, Chongqing University of Arts and Sciences, Chongqing 402160, People's Republic of China
[c] College of Physics, Chongqing University, Shapingba, Chongqing 401331, People's Republic of China
[d] State Key Laboratory of Luminescence and Applications, Changchun Institute of Optics, Fine Mechanics and Physics, Chinese Academy of Sciences, Changchun, Jilin Province 130033, People's Republic of China

ARTICLE INFO

Keywords:
ZnO
Multiple-step annealing
P-type conductivity
Intrinsic defects

ABSTRACT

The intrinsic defects in ZnO:In-N films can be regulated efficiently by multiple-step annealing together with the ambient atmosphere. Correspondingly, the conductivity of films changes from *n* to *p*-type, then to *n*-type ($n \rightarrow p \rightarrow n$). The experimental results indicate high-quality films annealed at 600 °C for 8 min in N_2 ambience can be obtained by the analysis of X-ray diffraction (XRD) patterns and the concentrations of donor defects (Zn_i, V_O) are dramatically decreased from Raman and photoluminescence (PL) spectra. When the films are further annealed in air for 3 min, the concentrations of acceptors such as oxygen interstitials (O_i) are increased slightly. Meanwhile, N-related acceptor complexes in the films are dominantly activated in terms of relative X-ray photoelectron spectroscopy (XPS) peak area ratio of P_1 (395.5 eV) and P_2 (397.3 eV) to P_3 (403.5 eV), which plays an important role in realizing the conversion of the ZnO *p*-type conductivity. Noted that the *p*-type ZnO:In-N films with the hole concentration of 10^{17} cm^{-3} can be obtained in this way.

1. Introduction

The direct semiconductor material ZnO with a wide bandgap of 3.37 eV has received extensively research attention due to the abundance of properties and functionalities over 20 years [1]. Compared with the GaN, ZnO has a larger free exciton binding energy (60 meV) and better optical response in the deep ultraviolet region that ensures it to be a promising candidate in the field of optoelectronics, such as ultraviolet light-emitting diodes (LEDs), ultraviolet (UV) detectors, photoelectrochemical sensor and solar cell [2–7].

As-grown ZnO frequently exhibits high levels of unintentional *n*-type conductivity with an electron concentration of the order 10^{17} cm^{-3} due to certain native point defects (Zn_i, V_O) that form spontaneously [8,9]. And the isolated Zn_i (double donor) can be created under nonequilibrium conditions such as irradiation, incorporating additional atoms or defects [10,11]. Even more important is that the formation energies of these defects (Zn_i, V_O) in the *p*-type ZnO (2.07, 0.73 eV) are lower than that of *n*-type one (5.45, 4.11 eV) [12,13], and their formation energies decrease rapidly with the Fermi level toward the valence-band maximum (VBM) [10]. Therefore, how to suppress intrinsic donor defects has become a hot issue in *p*-type doping of ZnO. Zn_i is theoretically expected to have an activation energy for self-diffusion of only 0.25 ~ 0.75 eV in good agreement with recent experimental data from low-temperature irradiation experiments [14,15], indicating that the concentrations of Zn_i can be tuned by post-annealing temperature. Moreover, the incorporation of isovalent atoms, like Cd [16], Mg [17], and Te [18], can influence the formation of the Zn_i related donors. Although the experimental investigations show that V_O can be suppressed significantly under O-rich condition [19–21], for N ion implantation into as-grown ZnO, a number of oxygen vacancies are so desirable due to the larger electronegativity (3.50) of the oxygen atom than the nitrogen atom (3.04) that the interstitial N (N_i) atoms energetically prefer to occupy oxygen vacancies to form N_O acceptors through post-annealing [22,23]. Generally, one main reason for unstable *p*-type conductivity of ZnO presumably may be the susceptibility of the acceptor complexes to environmental conditions. Obviously, the post-annealing in one step is difficult to achieve expectations that the forming acceptor complexes perform at the best [5,24]. Similar to *in-*

* Corresponding author.
E-mail address: qingp206@163.com (G. Qin).

https://doi.org/10.1016/j.apsusc.2020.146933
Received 21 April 2020; Received in revised form 2 June 2020; Accepted 6 June 2020
Available online 12 June 2020
0169-4332/

situ annealing, an innovative method of multiple-step rapid thermal annealing (RTA) was proposed. Here, the annealing parameters (such as temperature, time and atmosphere) are constantly adjusted by analysis of XRD and Hall measurements.

In this paper, the ZnO:In-N thin films were obtained by radio frequency magnetron sputtering and ion implantation. We deeply investigated the effect of multiple-step annealing on structure, optical and electrical properties of ZnO:In-N thin films by XRD, PL, Raman and XPS spectra, and better explained the *p*-type formation mechanism of ZnO films.

2. Experimental details

The ZnO:In-N films were prepared on quartz substrates by RF magnetron sputtering and multiple nitrogen ion implantations. The quartz substrates were ultrasonically cleaned with ethyl alcohol, acetone and deionized water in sequence for 10 min, and then transferred to the sputtering chamber immediately after drying with N_2. A commercial ZnO ceramic target with an indium content of 0.5 wt% was selected to the sputtering target. The sputtering chamber was evacuated to a base pressure of 5×10^{-4} Pa and argon (99.999%) was used as the sputtering gas with a constant pressure of 2 Pa. Moreover, the optimized parameters of gas flow rate, sputtering power and deposition time were 120 sccm, 120 W, and 45 min, respectively, based on our previous researches [17,24]. To create an approximately uniform profile of the implanted N ions within a certain depth (seen in Fig. S1), the as-deposited indium doped ZnO samples were subjected to N ions implantation with the energies of 130 keV (dose of 2×10^{16} cm^{-2}), 80 keV (dose of 8×10^{16} cm^{-2}), and 30 keV (dose of 2×10^{16} cm^{-2}), respectively. Finally, the ZnO:In-N films were annealed in a tube furnace. The multiple-step annealing included the first-stage annealing in a high-purity N_2 atmosphere at 600 °C for 8 min and several annealing stages (in air at 600 °C for 3 min). The following several annealing stages depend on the test results, which makes it possible to study the effect of "process scanning" annealing on the defects in ZnO:In-N films.

The thickness of the ZnO:In-N films measured by AMBIOS XP-1 surface profile was about 450 nm. The electrical properties were tested by the Hall Effect measurement (Ecopia HMS-3000) at room temperature, where eutectic Ga-In alloy ($\Phi_{In/Ga}$ = 4.12 eV) was used as electrode to ensure good ohmic contact with the surface of ZnO:In-N (Φ_{ZnO} = 4.3 eV) films (seen in Fig. S2). The crystal structure was characterized by XRD with Cu Kα1 as the emission source (λ = 1.540598 Å). Raman scattering and photoluminescence measurements were carried out in a test system (HR-800, JY Labram) using a semiconductor laser (λ = 532 nm) and a He-Cd laser (λ = 325 nm) as excitation sources respectively. The chemical state of nitrogen in ZnO:In-N films was detected by XPS and the binding energy was calibrated by the C1s peak at 285 eV.

3. Results and discussion

Fig. 1 shows the electrical properties of ZnO:In-N films annealed at different stages ($T_1 \sim T_3$). Firstly, the films annealed at 600 °C for 8 min in N_2 ambience (T_1) present a good *n*-type conductivity, corresponding electron concentration and resistivity are 2.13×10^{18} cm^{-3} and 4.03 Ω•cm, respectively. Subsequently, the films are annealed in air for 3 min (T_2), the conductivity changes into *p*-type. As the films are subjected to periodic repetition of the second stage annealing, the films still show *p*-type conductivity. The electrical properties of some samples with the same thermal treatment are listed in Table 1. Its corresponding hole concentration ranges from 1.45×10^{16} to 3.02×10^{17} cm^{-3}. In addition, the conversion from *p* to *n*-type conductivity happens with longer annealing time such as $t \geq 20$ min (T_3).

Fig. 2(a) illustrates the XRD patterns of ZnO:In-N films annealed at different stages as well as the as-implanted one. The samples have a c-axis preferred orientation because of the single (0 0 2) diffraction peak.

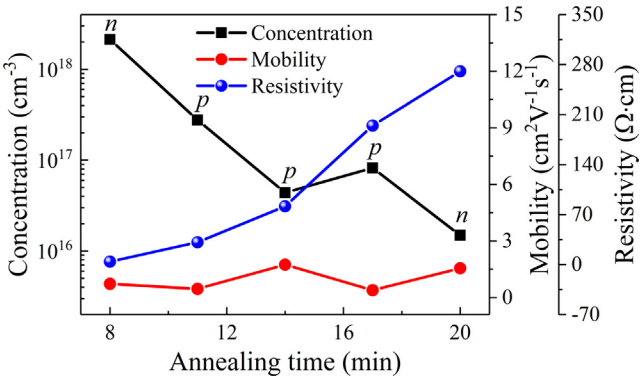

Fig. 1. (Color online) Electrical properties of ZnO:In-N films annealed at different stages.

Table 1
The electrical properties of *p*-type ZnO:In-N films.

Samples	Hole concentration(cm^{-3})	Mobility($cm^2V^{-1}s^{-1}$)	Resistivity (Ω•cm)	Type
A	1.54×10^{17}	0.84	48.27	*p*
B	1.45×10^{16}	2.65	162.4	*p*
C	2.06×10^{17}	1.82	16.65	*p*
D	3.02×10^{17}	0.59	34.90	*p*

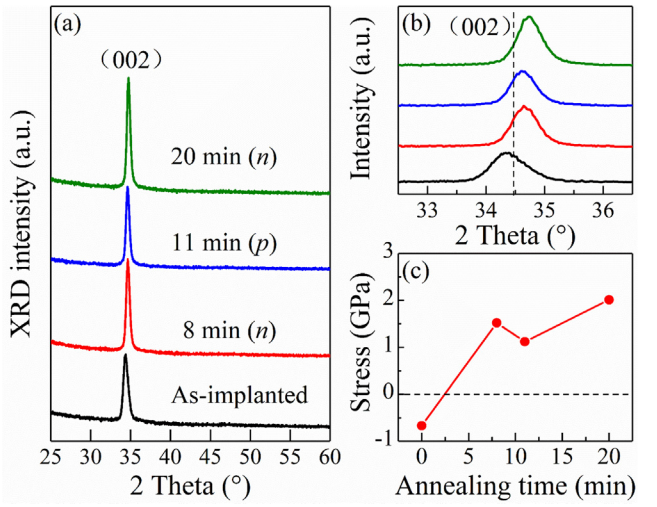

Fig. 2. (Color online) (a) XRD pattern of ZnO:In-N films annealed at different stages, (b)the shift of (0 0 2) diffraction peak with annealing time, (c) the variation of stress in ZnO:In-N films.

The diffraction peak of the films annealed at 600 °C in high purity N_2 ambience (II) is obviously higher than that of as-implanted (T_0), indicating the crystal structure has been improved greatly. Fig. 2(b) shows the local amplification of the (0 0 2) peak. One can see that the (0 0 2) peak of ZnO:In-N films compared to as-grown ZnO:In film (34.46°) shifts firstly to a lower angle then to the higher one with sequential annealing. Based on the biaxial strain model [25], the stress σ parallel to the films surface is calculated [see Fig. 2(c)]. The negative, positive values represent compressive and tensile stress in the film, respectively. For as-implanted ZnO:In-N film, the stress σ is is calculated to be −0.67 GPa, meaning strong compressive stress induced by abundant N interstitials (N_i). As the film is annealed at T_1 stage, the generation of tensile stress (1.53 GPa) are mainly attributed to the escaping of amounts of N_2 interstitial $(N_2)_i$ from N_i clustering under coulomb repulsion and N substitutions on vacancies. With the annealing time further increasing by 3 min in air (T_2), a slight decrease in

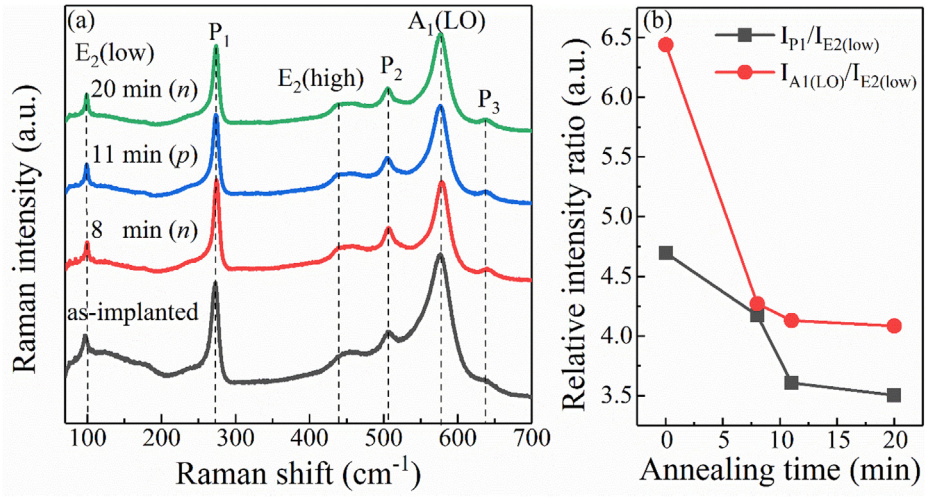

Fig. 3. (Color online) (a) Raman spectra of ZnO:In-N film with annealing time, (b) the ratio of the relative intensity of P_1 to E_2 (low)

tensile stress indicates that most of the oxygen vacancies may be occupied by N_i and ambient oxygen, which is consistent with the better *p*-type conductivity analysis given above. Noted that tensile stress up to 2.01 GPa means some nitrogen or oxygen atoms displace from lattice sites at T_3 stage.

Fig. 3(a) shows the Raman spectra of ZnO:In-N films annealed at different stages. The Raman spectra of the films contain six vibrational modes at 100, 275, 445, 505, 576 and 638 cm^{-1} in the range of 80–700 cm^{-1}. The vibrational modes occur at 100 and 445 cm^{-1} attribute to the low frequency and high frequency vibration of E_2 mode in ZnO, respectively, indicating the ZnO:In-N films have a wurtzite structure. The Raman mode at 576 cm^{-1} is usually associated with intrinsic defects (Zn_i, V_O) or their complexes in ZnO [26–27], while three additional modes at 275 (P_1), 505 (P_2) and 638 cm^{-1} (P_3) are induced by the N ions implantation [28]. Noted that the mode at 275 cm^{-1} was confirmed to be the vibration of small Zn_i clusters according to the comparative analysis of Zn isotope [29], indicating the implanted N ions can induce a certain amount of Zn_i in ZnO:In-N films.

To further understand the effects of multiple-step annealing on intrinsic defects (Zn_i, V_O), $I_{P1}/I_{E2\ (low)}$ and $I_{A1(LO)}/I_{E2(low)}$ are used to represent the normalized intensity of the 275 and 576 cm^{-1} modes, as shown in Fig. 3(b). In contrast with as-implanted samples, the $I_{P1}/I_{E2\ (low)}$ of the films annealed for 8 min in high purity N_2 ambience (T_1) decreases from 4.7 to 4.2, indicating some Zn_i clusters may be dissociated and a few Zn_i diffuse out of the surface [30]. The same trend in $I_{A1(LO)}/I_{E2(low)}$ indicates that the concentration of oxygen vacancies may decrease significantly due to the substitution of N_i for V_O. As the annealing time is extended for another 3 min in air (T_2), both $I_{P1}/I_{E2\ (low)}$ and $I_{A1(LO)}/I_{E2(low)}$ decrease to some extent, which is in favor of the conversion of *p*-type conductivity in ZnO films. Noted that a certain amount of Zn_i or/and V_O still remain in the ZnO:In-N films by several annealing cycles (T_3) from the analysis of Raman spectra.

Photoluminescence is a quite sensitive measurement to investigate the evolution of intrinsic defects during the thermal treatment. As shown in Fig. 4, the PL spectra of the films are mainly composed of the near band edge emission (P_1) and the broad visible emission region. The broad emission can be divided into five peaks at about 450, 520, 558, 592 and 633 nm by Gaussian fitting. The blue emission peak P_2 at 430 ~ 450 nm is usually considered to an electron transition from Zn_i to valance band maximum in the ZnO [31–33]. The yellow-green emission usually is attributed to the recombination of deep defects state located inside the band gap. The emission ranging at 500 ~ 590 nm presumably results from a transition of an electron from near conduction band edge to a deeply trapped hole in V_O^+ or V_O^{2+} of the ZnO [34–35]. So far, many research groups have agreed that the emissions are closely related

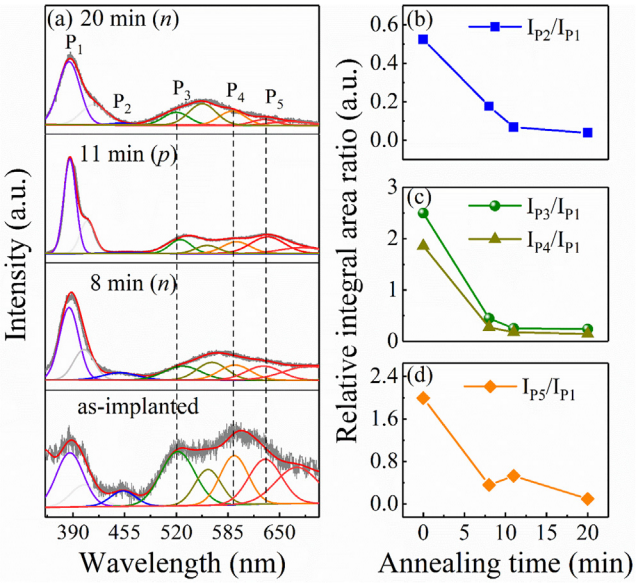

Fig. 4. (Color online) (a) PL spectra of ZnO:In-N film with annealing time, (b-d) the variation of the relative intensity of intrinsic defects (Zn_i, V_O, and O_i).

to the V_O [36–39]. In addition, the O_i or adsorbed oxygen is identified as responsible for the emission of 633 nm [40–41].

Fig. 4(b-d) shows the relative integral area ratio of the emission peaks (P_2, P_3, P_4 and P_5) to NBE. It can be clearly seen the relative ratios of the P_2, P_3 and P_4 constantly decreased during the thermal treatment, indicating the gradual decrease of the concentration of Zn_i and V_O. Especially, the films further annealed in air maintain donor defects (Zn_i, V_O) at low concentrations. It can be explained as follows: As the ZnO polycrystalline films prepared by magnetron sputtering are annealed at T_1 stage, the amounts of Zn_i induced by the implanted N ions can diffuse to the surface of grain boundaries (GBs). Subsequently, the films are further annealed at 600 °C for 3 min in air (T_2), ambient oxygen diffuses easily along GBs and interacts with Zn_i adjacent to the surface of GBs, accompanied by the formation of a thin high-resistance layer on the surface of GBs [42,43]. Meanwhile, excess amounts of oxygen can occupy V_O or interstitial sites. All these may contribute to the conversion of *p*-type conductivity of ZnO:In-N films.

To further understand the role of N impurity in formation mechanism of *p*-type ZnO:In–N films, the investigation into the chemical bonding state of N is necessary by XPS. The peak at 403.5 eV (P_3) arises from the N-N bond because N_i has the tendency of clustering in ZnO

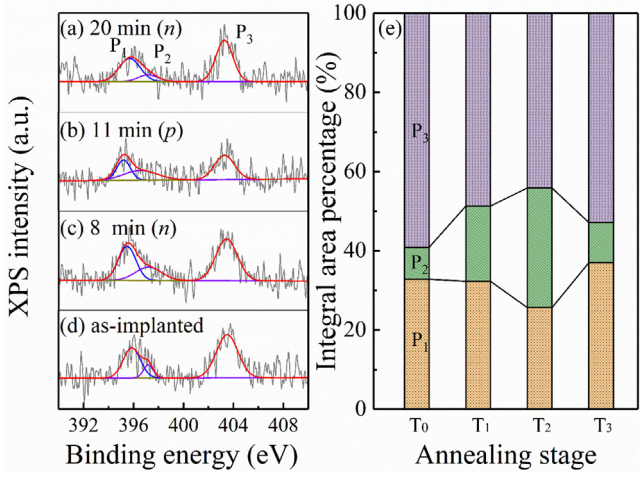

Fig. 5. (Color online) (a-d) N 1 *s* XPS for ZnO:In-N films, (e) the integral area percentage of P_1, P_2 and P_3.

under coulomb repulsion [44]. The broad spectral peaks ranging from 394.1 to 398.3 eV can be disassembled into two peaks centered at 395.5 eV (P_1) and 397.3 eV (P_2) by Gaussian fitting. The binding energy at 396.5 eV is definitely assigned to the formation of N–Zn bond [45]. According to the electronegativity sequence ($\chi_{Zn} < \chi_{In} < \chi_N$), the relations of bonding energy in ZnO:In-N films as follows: E_b(Zn - N) < E_b(In - N) < E_b(N - N). Therefore, the P_2 more likely originates from Zn-N bond where part of Zn atoms were replaced by In atoms [24]. To compare the relative intensity of N-related defects in ZnO:In-N films annealed at different stages, the integral area percentages of the three components for N 1 s XPS are presented in Fig. 5(e). It is clear that the integral area percentages of P_1 and P_2 are dominant in the case of the films annealed at T_2 stage, which indicates the abundant N ions can occupy V_O to form N_O acceptors during the thermal treatment. Correspondingly, the content of intrinsic donor defects (Zn_i, V_O) is less, but that of acceptor defects (O_i) in the films is more. Accordingly, the complexes of N_O and intrinsic acceptor defects are responsible for the *p*-type conductivity. Once the films are annealed at T_3 stage, the intensity sum of P_1 and P_2 decrease slightly due to the displacement of N atoms from their lattice sites, causing that the *p*-type conductivity of ZnO:In-N films convert into *n*-type again.

4. Conclusions

The ZnO:In-N films on quartz substrates by RF magnetron sputtering and multiple nitrogen ions implantation were fabricated. And the impact of multiple-step annealing on the physical properties of the films has been deeply investigated. The XRD results show that the crystal structure damaged by ions implantation can be greatly recovered by annealing at 600 °C, and the corresponding stress changes gradually from large compressive stress into slight tensile stress. The Hall Effect measurements imply that the conductivity of the ZnO:In-N thin films by multiple-step annealing together with the ambient atmosphere presents the characteristics of $n \rightarrow p \rightarrow n$. During annealing in air (T_2), the amounts of Zn_i defects are reduced and a few O_i are created from the Raman and PL spectra. Noted that the N-related acceptors dominantly activated and a number of O_i defects formed collectively contribute to *p*-type conductivity of the ZnO:In-N thin films. However, as the annealing time increases too much (20 min), the films behave as *n*-type conductivity again due to the diminishing of the acceptor defects. Moreover, the experimental results verify that the reliable *p*-type ZnO films can be realized repeatedly by our proposed procedure.

CRediT authorship contribution statement

Xiaoyu Zhang: Writing - original draft. **Guoping Qin:** Methodology. **Hong Zhang:** Visualization, Investigation. **Wanjun Li:** Data curation. **Haibo Ruan:** Software. **Liang Fang:** Methodology. **Cunzhu Tong:** Conceptualization. **Chunyang Kong:** Supervision.

Declaration of Competing Interest

The authors declare that they have no known competing financial interests or personal relationships that could have appeared to influence the work reported in this paper.

Acknowledgements

The authors gratefully acknowledge support from the National Natural Science Foundation of China (Grant Nos. 11904041, 51472038 and 51502030), the Nature Science Foundation of Chongqing City (Grant Nos. CSTC2016jcyjA, 2018jcyjA2923), State Key Laboratory of Luminescence and Applications (SKLA-2020-10), the Dr. Scientific Research Fund (Grant Nos. 16XlB002, 20XlB002) and Postgraduate Research Innovation Project (Grant No.YKC19017) of Chongqing Normal University.

Appendix A. Supplementary data

Supplementary data to this article can be found online at https://doi.org/10.1016/j.apsusc.2020.146933.

References

[1] D.M. Bagnall, Y.F. Chen, Z. Zhu, T. Yao, S. Koyama, M.Y. Shen, T. Goto, Optically pumped lasing of ZnO at room temperature, Appl. Phys. Lett. 70 (1997) 2230–2232.
[2] D. Zheng, G. Wang, W. Huang, B. Wang, W. Ke, J.L. Logsdon, H. Wang, Z. Wang, W. Zhu, J. Yu, M.R. Wasielewski, M.G. Kanatzidis, T.J. Marks, A. Facchetti, Combustion synthesized zinc oxide electron-transport layers for efficient and stable perovskite solar cells, Adv. Funct. Mater. 29 (2019) 1900265.
[3] Y.J. Lu, Z.F. Shi, C.X. Shan, D.Z. Shen, ZnO-based deep-ultraviolet light-emitting devices, Chinese. Phys. B 26 (2017) 047703.
[4] A. Liu, K. Yin, L. Mi, M. Ma, Y. Liu, Y. Li, W. Wei, Y. Zhang, S. Liu, A novel photoelectrochemical immunosensor by integration of nanobody and ZnO nanorods for sensitive detection of nucleoside diphosphatase kinase-A, Anal. Chim. Acta. 973 (2017) 82–90.
[5] A. Purohit, S. Chander, A. Sharma, S.P. Nehra, M.S. Dhaka, Impact of low temperature annealing on structural, optical, electrical and morphological properties of ZnO thin films grown by RF sputtering for photovoltaic applications, Opt Mater. 49 (2015) 51–58.
[6] R.X. Wang, L.C. Yang, Y.M. Zhang, S.J. Xu, K. Fu, B.S. Zhang, J.F. Wang, K. Xu, H. Yang, The effect of Ga-doped nanocrystalline ZnO electrode on deep-ultraviolet enhanced GaN photodetector, Appl. Phys. Lett. 102 (2013) 212104.
[7] Ü. Özgür, Y.I. Alivov, C. Liu, A. Teke, M.A. Reshchikov, S. Doğan, V. Avrutin, S.J. Cho, H. Morkoç, A comprehensive review of ZnO materials and devices, J. Appl. Phys. 98 (2005) 041301.
[8] K.E. Knutsen, A. Galeckas, A. Zubiaga, F. Tuomisto, G.C. Farlow, B.G. Svensson, A.Y. Kuznetsov, Zinc vacancy and oxygen interstitial in ZnO revealed by sequential annealing and electron irradiation, Phys. Rev. B 86 (2012) 121203.
[9] M.D. McCluskey, S.J. Jokela, Defects in ZnO, J. Appl. Phys. 106 (2009) 071101.
[10] A. Janotti, C.G. De Walle, Native point defects in ZnO, Phys. Rev. B 76 (2007) 165202.
[11] L.S. Vlasenko, G.D. Watkins, Optical detection of electron paramagnetic resonance for intrinsic defects produced in ZnO by 2.5-MeV electron irradiation in situ at 4.2 K, Phys. Rev. B 76 (2005) 035203.
[12] R. Vidya, P. Ravindran, H. Fjellvåg, B.G. Svensson, E. Monakhov, M. Ganchenkova, R.M. Nieminen, Energetics of intrinsic defects and their complexes in ZnO investigated by density functional calculations, Phys. Rev. B 83 (2011) 045206.
[13] K. Tang, S.L. Gu, J.D. Ye, S.M. Zhu, R. Zhang, Y.D. Zheng, Recent progress of the native defects and p-type doping of zinc oxide, Chinese. Phys. B 26 (2017) 047702.
[14] P. Erhart, K. Albe, Diffusion of zinc vacancies and interstitials in zinc oxide, Appl. Phys. Lett. 88 (2006) 201918.
[15] C. Bhoodoo, A. Hupfer, L. Vines, E.V. Monakhov, B.G. Svensson, Evolution kinetics of elementary point defects in ZnO implanted with low fluences of helium at cryogenic temperature, Phys. Rev. B 94 (2016) 205204.
[16] W. Li, L. Fang, G. Qin, H. Ruan, H. Zhang, C. Kong, L. Ye, P. Zhang, F. Wu, Tunable zinc interstitial related defects in ZnMgO and ZnCdO films, J. Appl. Phys. 117 (2015) 145301.
[17] H. Zhang, W. Li, G. Qin, H. Ruan, Z. Huang, F. Wu, C. Kong, L. Fang, Role of zinc

interstitial defects in indium and magnesium codoped ZnO transparent conducting films, Appl. Surf. Sci. 492 (2019) 392–398.
[18] K. Tang, R. Gu, S. Gu, J. Ye, S. Zhu, Z. Yao, Z. Xu, Y. Zheng, Annealing in tellurium-nitrogen co-doped ZnO films: The roles of intrinsic zinc defects, J. Appl. Phys. 117 (2015) 135304.
[19] D.A. Tomoyuki Kawashima, Katsuyoshi Washio, Investigation on a source of dominant donor in vanadium-doped ZnO films grown by reactive RF magnetron sputtering, Mat. Sci. Semicon. Proc. 70 (2017) 213–218.
[20] M.E. FragalÃ, G. Malandrino, M.M. Giangregorio, M. Losurdo, G. Bruno, S. Lettieri, L.S. Amato, P. Maddalena, Structural, optical, and electrical characterization of ZnO and Al-doped ZnO thin films deposited by MOCVD, Chem. Vapor. Depos. 15 (2009) 327–333.
[21] S.B. Zhang, S.H. Wei, A. Zunger, Intrinsicn-type versusp-type doping asymmetry and the defect physics of ZnO, Phys. Rev. B 63 (2001) 075205.
[22] W. Li, C. Kong, H. Ruan, G. Qin, L. Fang, X. Meng, H. Zhang, P. Zhang, Q. Xu, Investigation on the formation mechanism of In–N codoped p-Type ZnCdO thin films: experiment and theory, J. Phys. Chem. C 118 (2014) 22799–22806.
[23] T.M. Børseth, F. Tuomisto, J.S. Christensen, E.V. Monakhov, B.G. Svensson, A.Y. Kuznetsov, Vacancy clustering and acceptor activation in nitrogen-implanted ZnO, Phys. Rev. B. 77 (2008) 045204.
[24] G.P. Qin, H. Zhang, W.J. Li, H.B. Ruan, J. Wang, D. Wang, L. Fang, C.Y. Kong, Investigation on the formation mechanism of p-type ZnO:In-N thin films: experiment and theory, J. Mater. Sci-Mater. El. 30 (2019) 6059–6064.
[25] K. Bahedi, M. Addou, M.E. Jouad, Z. Sofiani, H.E. Oauzzani, B. Sahraoui, Influence of strain/stress on the nonlinear-optical properties of sprayed deposited ZnO: Al thin films, Appl. Surf. Sci. 257 (2011) 8003–8005.
[26] C.J. Youn, T.S. Jeong, M.S. Han, J.H. Kim, Optical properties of Zn-terminated ZnO bulk, J. Cryst. Growth. 261 (2004) 526–532.
[27] J.M. Liu, C.K. Ong, L.C. Lim, Pulsed laser deposition of ZnO as conductive buffer layer of (001)-$LiNbO_3$ thin films, Ferroelectrics 231 (1999) 223–229.
[28] J.B. Wang, H.M. Zhong, Z.F. Li, W. Lu, Raman study of N^+-implanted ZnO, Appl. Phys. Lett. 88 (2006) 101913.
[29] M.A. Gluba, N.H. Nickel, N. Karpensky, Interstitial zinc clusters in zinc oxide, Phys. Rev. B 88 (2013) 245201.
[30] K. Tang, R. Gu, S. Zhu, Z. Xu, J. Ye, S. Gu, Thermal evolution of zinc interstitial related donors in high-quality NH_3-doped ZnO films, Opt. Mater. Express. 7 (2017) 593–605.
[31] H. Shen, X. Zhao, L. Duan, R. Liu, H. Li, B. Wang, Effect of Na_{Zn}/Na_i ratio on structural, optical, and electrical properties of Na-doped ZnO thin films, J. Appl. Phys. 121 (2017) 155303.
[32] C. Jayachandraiah, K.S. Kumar, G. Krishnaiah, N.M. Rao, Influence of Dy dopant on structural and photoluminescence of Dy-doped ZnO nanoparticles, J. Alloy. Compd. 623 (2015) 248–254.
[33] L. Duan, X. Zhao, Y. Wang, H. Shen, W. Geng, F. Zhang, Influence of Cd doping on structural and optical properties of (Cd, Al)-codoped ZnO powders synthesized via sol–gel method, J. Alloy. Compd. 645 (2015) 529–534.
[34] K. Vanheusden, W.L. Warren, C.H. Seager, D.R. Tallant, J.A. Voigt, B.E. Gnade, Mechanisms behind green photoluminescence in ZnO phosphor powders, J. Appl. Phys. 79 (1996) 7983–7990.
[35] A.V. Dijken, E.A. Meulenkamp, D. Vanmaekelbergh, A. Meijerink, The kinetics of the radiative and nonradiative processes in nanocrystalline ZnO particles upon photoexcitation, J. Phys. Chem. B 104 (2000) 1715–1723.
[36] Y. Xu, H. Li, B. Sun, P. Qiao, L. Ren, G. Tian, B. Jiang, K. Pan, W. Zhou, Surface oxygen vacancy defect-promoted electron-hole separation for porous defective ZnO hexagonal plates and enhanced solar-driven photocatalytic performance, Chem. Eng. J. 379 (2020) 122295.
[37] Y.P. Xie, Y. Yang, G. Wang, G. Liu, Oxygen vacancies promoted interfacial charge carrier transfer of CdS/ZnO heterostructure for photocatalytic hydrogen generation, J. Colloid. Interf. Sci. 503 (2017) 198–204.
[38] C. Zou, F. Liang, S. Xue, Synthesis and oxygen vacancy related NO_2 gas sensing properties of ZnO: Co nanorods arrays gown by a hydrothermal method, Appl. Surf. Sci. 353 (2015) 1061–1069.
[39] J. Su, C. Wang, C. Tang, Q. Niu, Y. Zhang, Z. Fu, Influence of annealing on the structural and optical properties of ZnO films grown by MOCVD, J. Alloy. Compd. 509 (2011) 6102–6105.
[40] J.A. Röhr, J. Sá, S.J. Konezny, The role of adsorbates in the green emission and conductivity of zinc oxide, Commun. Chem. 2 (2019) 1–7.
[41] V. Kumar, H.C. Swart, O.M. Ntwaeaborwa, R.E. Kroon, J.J. Terblans, S.K.K. Shaat, A. Yousif, M.M. Duvenhage, Origin of the red emission in zinc oxide nanophosphors, Mater. Lett. 101 (2013) 57–60.
[42] Y.J. Kim, H.J. Kim, Trapped oxygen in the grain boundaries of ZnO polycrystalline thin films prepared by plasma-enhanced chemical vapor deposition, Mater. Lett. 41 (1999) 159–163.
[43] V. Nosenko, N. Korsunska, I. Vorona, T. Stara, V. Bondarenko, O. Melnichuk, L. Melnichuk, A. Kryvko, I. Markevich, The mechanism of formation of interface barriers in ZnO: Mn ceramics, SN Applied Sciences 2 (2020) 1–5.
[44] S. Limpijumnong, X. Li, S.H. Wei, S.B. Zhang, Substitutional diatomic molecules NO, NC, CO, N_2, and O_2: Their vibrational frequencies and effects on p doping of ZnO, Appl. Phys. Lett. 86 (2005) 211910.
[45] N. Tabet, M. Faiz, A. Al-Oteibi, XPS study of nitrogen-implanted ZnO thin films obtained by DC-Magnetron reactive plasma, J. Electron. Spectrosc. 163 (2008) 15–18.